A Novel Induction Heating Fluidized Bed Reactor: Its Design and Applications in High Temperature Screening Tests with Solid Feedstocks and Prediction of Defluidization State

Mohammad Latifi and Jamal Chaouki
Dept. of Chemical Engineering, Ecole Polytechnique de Montreal, C.P. 6079, Succ. Centre-ville, Montreal, QC, Canada, H3C 3A7

DOI 10.1002/aic.14749
Published online March 6, 2015 in Wiley Online Library (wileyonlinelibrary.com)

A novel mini induction heating fluidized bed reactor (IHFBR) is introduced which was developed to carry out screening tests of high temperature reactions up to 1500°C particularly for solid feedstocks. Despite conventional mini reactors, this reactor mimics real scenario of solid feeding in industrial reactors: cold feedstock is injected within 1 s from a lift tube, then particles reach reaction temperature in less than 5 s in a reaction zone. The lift tube (9.5 cm diameter) is also the gas distributor of the fluidized bed (2.5 cm diameter) so that the bed is completely fluidized with uniform gas distribution. Beside facilities to perform tests in a fluidized bed, another important feature of this reactor is prediction of the defluidization state in the bed. Not only reproducible data are generated, but also many tests can be conveniently carried out, that is, one test per hour. © 2015 American Institute of Chemical Engineers *AIChE J*, 61: 1507–1523, 2015
Keywords: induction heating, fluidization, lift tube, coal combustion, defluidization

Introduction

Pilot plant reactors offer very important advantages in testing operating conditions such as temperature, pressure, residence time, catalyst to feed ratio, instrumentation and so on. However, such units are very costly when used, for example, for catalyst and feedstock screening tests where many tests are required to find out effect of new formulations on product yield under different operating conditions.[1] Small-scale reactors are, conversely, ideal equipment for such purposes as with such systems running an operation is not expensive, performing a test does not take significant time, switching from an operating condition to one another is rather quick and above all, mass of required catalyst and feedstock is small, that is, in the order of grams. Therefore, considerable time and cost is saved through running tests in the small-scale reactors.

There are some challenges in designing and operation of the small-scale reactors to mimic reaction conditions in the industrial fluidized bed reactors properly,[2,3] in particular, when the feedstock is a solid. Some of these challenges include supply of the required heat, gas residence time, feeding technique and effective gas-solid contact.

In particular, these issues are found in the traditional fixed bed mini reactors; an example of such fixed bed reactors is the conventional Thermo Gravimetric Analyzer (TGA). TGAs are widely used for many applications in which mass of a solid feedstock is placed inside a crucible; then while being on a scale, the crucible is heated by an external heater. Due to flow of gas passing over the top of the crucible, diffusion of gas into bulk and into grains of the solid feedstock control rate of interaction between gas and solid.[4] Also, since heat is transferred from crucible into the solid feedstock, there is a temperature gradient within bulk of the solid feedstock; that is, temperature in the wall of the crucible is larger than temperature in its middle. In addition, there is no means to enhance gas-solid contact by mixing, and achievable heating rate is limited. The novel fluidized bed TGA overcomes diffusion limitations in the conventional fixed bed TGAs,[5] but there are still heating rate limitations.

There are other fluidized bed test reactors for tests with the solid feedstock that improve mixing while they have heating rate limitations. As a matter of the fact, in industrial high temperature fluidized bed reactors a cold solid feedstock is injected to a hot bed. Then, duration of complete reaction of the feedstock is a function of its composition, mass and particle-size distribution as well as type of the reactant gases. In such cases, because mass of the bed inventory is considerably higher than mass of the feedstock, temperature drop is not significant in the bed and particles of the solid feedstock quickly, that is, within some seconds reach temperature of the reactor.

Conversely, available mini reactors cannot truly mimic this phenomenon. Therefore, as soon as a feedstock is injected: thermal or catalytic reaction starts to proceed and bed temperature drops while there is a temperature difference between the bed and the feedstock. As a result, the obtained data of feed conversion and concentration of product gases are erroneous.

This crucial weakness is due to slow heating rate in the present mini fluidized bed reactors, which use external heaters. In such cases, a significant portion of the radiated heat

Corresponding concerning this article should be addressed to J. Chaouki at jamal.chaouki@polymtl.ca

Table 1. Comparison of Some Mini Fluidized Bed Reactors for High Temperature Reaction Tests

Mini reactor	FB-TGA[5]	Gas-solid MFBRA[6–8]	CLC fluidized bed[9–12]	SCTRT[13]	Riser simulator[14–16]
Bed inventory, (g)	30	3	45	12–24	1
Feed mass, (g)	0.1	0.001–0.075	Solid: 0.25–1 Liquid:1–2	3	0.13 (Feed is injected in the annulus)
Heating method	External furnace	External furnace	External furnace	External furnace	External furnace (bed is heated through gas circulation in the annulus)
Heating rate issues	Not discussed	Not discussed	Not discussed	Not discussed	Not discussed
Fluidization highlights	Diffusion effects are minimized in a bubbling bed TGA		Chemical looping combustion of liquid and solid fuels	Designed for FCC tests with overall vapor- catalyst contact time of 2 to 4 seconds	Fluid bed in an internal basket An internal impeller achieves gas flow
Fluidization dynamics	Not discussed	Not discussed	Not discussed	Not discussed	Not discussed

from the external heaters is lost to environment. In addition, the absorbed part of the radiated heat will be partly consumed to heat up whole mass of the reactor. As a result, there is a major response delay by the external heaters, which is sometimes in the order of some minutes.[6] This is a serious drawback, especially, in reactions like gasification and combustion where kinetics is in the order of seconds or milliseconds.

FB-TGA,[5] MFBRA,[6–8] CLC fluidized bed,[9–12] SCTRT,[13] and riser simulator[14–16] are mini fluidized bed reactors that are developed for different high temperature reactions with some features listed in Table 1. Although these reactors provide convenience to maintain certain operating conditions such as feed to bed mass ratio, residence time, and effective gas-solid contact, they all use a type of external heater to supply the required heat. It is noteworthy that heating rate limitations in such reactors are not discussed in references.

The induction heating fluidized bed reactor (IHFBR) was designed to exactly mimic the real scenario in industrial reactors by addressing the heating drawback in the preceding mini fluidized bed reactors. In this reactor, the required heat is supplied by induction heating mechanism; therefore, the reactor takes advantage of a high power heat generation inside the fluidized bed only, which helps solid particles reach the reaction temperature within a few seconds. This successful analogy is highly supported by a designed lift tube through which the solid feedstock is instantaneously and precisely fed to the hot fluidized bed of the reactor within a second while its temperature at the inlet of the bed is very low similar to the cases in industrial reactors. Performance of feeding is not discussed in the reactors in Table 1 that were used for solid feedstock handling; however, it is realized from the published descriptions that there should have been drawbacks with the used techniques. For instance, solid feed is injected to the annulus section of the riser simulator[16]; therefore, solid volatilization must occur first before vapors can have contact with the fluidized bed. Solid shooting with a gas through a 3 mm tubing is another technique that have been used in semi-batch mini fluidized bed reactors,[6,12] but there should be plugging issues with respect to particle-size distribution of the feedstock.

Another important feature of the lift tube is that in the absence of a porous or a perforated gas distributor, it is indeed the gas distributor of the IHFBR; in other words, exit gas from the lift tube is uniformly distributed in the hot fluidized bed. As presented in Table 1, fluidization quality is not often discussed in the conventional mini fluidized bed reactors. However, it was important to study quality of fluidization in the IHFBR to ensure uniform solid mixing is not deteriorated due to operation of the lift tube.

The IHFBR is a semi batch fluidized bed reactor which can operate at extremely high temperatures, that is, up to 1500°C. Tests with a solid feedstock such as coal, biomass, waste, and petroleum coke can be conducted in the reactor if particles are classified as the Geldarts' group A or group B powders. Depending on the tests, different inert, reductive, and oxidative gases can be used. This reactor can be used for screening tests and kinetic studies of endothermic and exothermic reactions such as thermal and catalytic cracking, pyrolysis, gasification, and combustion.

Induction Heating

True understanding of induction heating helps design an induction heating setup properly. Induction heating[17–19] is a noncontact, clean, repeatable, and fast heating method to

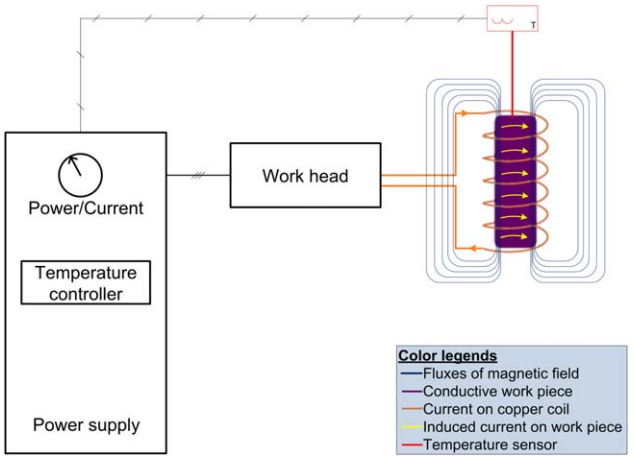

Figure 1. Schematic of an induction heating setup.

[Color figure can be viewed in the online issue, which is available at wileyonlinelibrary.com.]

heat up an electrically conductive material that is, work piece placed inside a strong magnetic field which alternates with a high frequency, f. The magnetic field induces eddy currents, I, flowing on the work piece; then, given each electrical conductive material has resistivity, r, against eddy currents, heat is generated, rI^2.

If a ferromagnetic work piece such as steel and nickel is heated by induction heating, heat is also generated due to hysteresis losses: as a matter of the fact, the dipoles of the ferromagnetic work piece have to get aligned with the poles of the magnetic field. Therefore, because of the alternative magnetic field and oscillation of its magnetic poles, the dipoles of the work piece oscillate accordingly; as a result, heat is generated due to friction between the dipoles. Hysteresis heat is generated until the Curie temperature is passed after which the ferromagnetic work piece is not magnetic any longer. Hysteresis loss is usually considered a minor heat source compared to eddy currents.

During induction heating, heat is mainly generated on the surface of the work piece, that is, reference depth, d, so its core remains relatively far less hot which helps eliminate risk of distorting it; this phenomenon is called skin effect. Within the reference depth, strength of the induced magnetic field, equivalent to intensity of eddy currents, is reduced by 86% starting from surface of the work piece. The reference depth depends on frequency of the electrical current, f, electrical resistivity, r, and relative magnetic permeability, μ, of the work piece as presented in Eq. 1

$$d = k\sqrt{\frac{r}{\mu f}} \quad , \quad k = \text{constant} \tag{1}$$

Depending on objective of the induction heating, selection of the frequency is of great importance for a given work piece. For instance, reference depth is thinner at very high frequencies while it is increased when frequency is lowered. Thus, if a through-heating of the work piece is required, lower frequencies should be applied in comparison with shallow heating where larger frequencies are required. Frequency in induction heating can vary between 5 and 500 kHz. Diameter of the work piece should be taken into account to select the right frequency because if diameter was small enough, eddy currents of either side of the work piece would impinge on each other and lead to a net zero current, and therefore, no heating will occur.

It is noteworthy that the length of the work piece which is placed inside the magnetic field is mainly heated by induction heating while the remaining part is heated by conduction heating which is much slower than induction heating; this advantage provides many applications for induction heating in hardening, brazing, and welding industries.

A schematic of the induction heating setup is shown in Figure 1. Essential elements of such unit are a power supply, a work head, a copper coil, and a work piece. The power supply generates a strong power by converting the input direct current to an output alternative current with high amperage and frequency. The work head acts as a transformer and transfers the alternative current from the power supply onto the copper coil.

The copper coil, inside which the work piece is located, is a very important part of the induction heating setup and is designed in different forms for each heating application in terms of number of turns and structural shapes. Intensity of magnetic field is the highest inside the coil. Despite the work piece which should have considerable electrical resistivity, copper is the main material to build the coil to minimize self heating the coil, especially because a large alternative current is passing through it. For the sake of safety of the coil, cooling water must always flow through inside the copper coil to prevent its melting and formation of soldered or brazed joints.

Thickness of the coil must be larger than its reference depths to let the electrical current flow, but it must be thin enough to be able to make the required shape of the coil conveniently and to accelerate heat transfer to cooling water.

Diameter of the coil must be as close as possible to diameter of the work piece to provide an efficient coupling between them and increase overall efficiency of the coil. This is important especially when frequency of the magnetic field is very high because in this case fluxes of the magnetic field tend to be close to the coil than to its center.

Temperature of the heated work piece can be measured by a temperature sensor such as a thermocouple or an infrared pyrometer. The thermocouple is cheaper and can be easily attached to the work piece to measure the temperature directly, but its response time is slow and its attachment to the work piece can be a challenge. Conversely, the infrared pyrometer is a fast responsive tool and does not require attachment to the work piece, but it has to see the hot spot correctly, otherwise, it can sense a completely wrong temperature.

Temperature has direct effect on the rate and efficiency of induction heating. For instance, the reference depth on the work piece is increased vs temperature; therefore, if its diameter is not large enough, the work piece could be heated at low temperatures, but induced current will be stopped upon reaching a certain temperature. As an example, as it will be seen later, a type K thermocouple with 1.6×10^{-3} m diameter is used in the IHFBR; investigations on interaction of the thermocouple in the magnetic field revealed that the thermocouple was heated by induction heating only until temperatures around 200°C. Bearing this advantage in mind, the read temperature above 200°C was assumed as the true temperature of the fluidized bed of the IHFBR.

Apparatus of Induction Heating Fluidized Bed Reactor

The new induction heating fluidized bed reactor (IHFBR) is designed for semicontinuous tests of extremely high

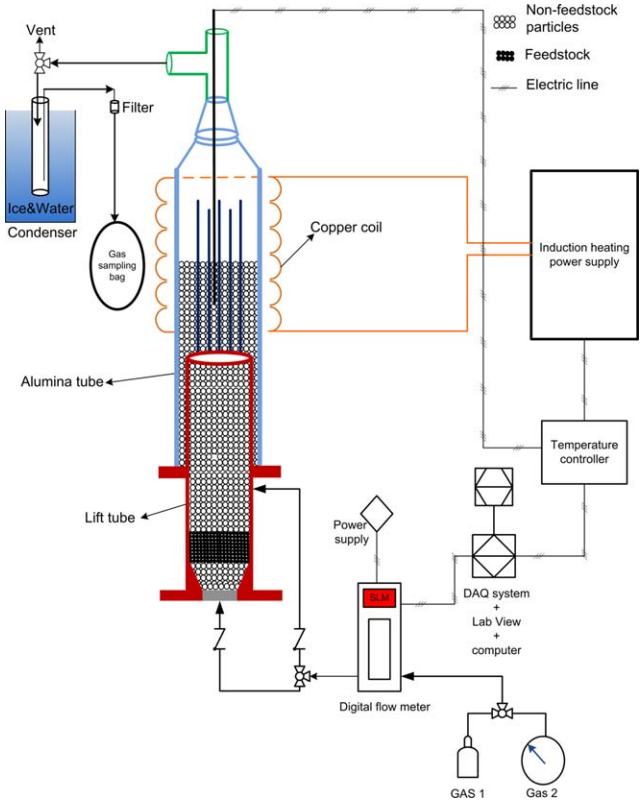

Figure 2. Setup of the Induction Heating Fluidized Bed Reactor (IHFBR); arbitrary dimensions are shown to better present the details.

[Color figure can be viewed in the online issue, which is available at wileyonlinelibrary.com.]

temperature reactions such as combustion, gasification, and pyrolysis. Operation flexibility for doing different experimental tests is an outstanding feature of the IHFBR; for instance, kinetic of chemical reactions and screening tests can be performed for solid feedstock such as biomass, coal, waste, and petroleum coke with either oxidative, reductive, or inert gases.

A schematic of the IHFBR's setup is presented in Figure 2. This setup is composed of two sections: reaction zone and lift tube.

The reaction zone is inside an alumina tube with 0.025 m diameter and 0.3 m length. The alumina tube is used because it is not electrically conductive, and therefore, it does not shield against magnetic field of the induction heating; also, it can safely withstand temperatures up to 1500°C. There are eight electrically conductive metal rods with 3.2 mm diameter and 0.1 m length inside the alumina tube, which are symmetrically placed on top of the lift tube. In fact, these rods are the work pieces of the induction heating system and they play the role of heating elements of the reactor. The top view schematic of the reaction zone presented in Figure 3 clarifies position of the metal rods in the bed, their relative distance and their distance with internal diameter of the alumina tube and internal diameter of the lift tube.

A 10 kW NORAX power supply generates the required power for induction heating. A coil with 0.038 m internal diameter and eight turns made of 6.4×10^{-3} m O.D. copper tubing is used to induce electrical current on the surface of the rods. The alumina tube is actually placed inside the coil. Depending on application, nonfeedstock solid particles such as silica sand are fluidized in the reaction zone. Mass of the solid particles is chosen so that expanded height of their bed is as high as length of the rods.

Depending on the required heating rate, the power is adjusted by a temperature controller and the rods are heated accordingly, then the generated heat on the surface of the rods is transferred to the fluidized bed inside-out toward the reactor wall. A type K thermocouple is used to read temperature of the bed. Since solid particles are being fluidized, temperature remains uniform in the bed; there is usually ± 10°C variation around the setpoint temperature which is normal in the fluidized beds. The temperature uniformity has been confirmed using two thermocouples on the top and on the bottom of the bed. It is noteworthy that an infrared pyrometer was initially used for temperature measurement for the sake of its fast response and noncontact features for precise temperature readings at extremely high temperatures, but there was one failing drawback with it: the actual hot spot must be seen by the infrared beams; otherwise, a wrong temperature will be read, especially, when there is a dark environment because of reactants and products.

The lift tube that has 0.15 m length and 9.5×10^{-3} m internal diameter is designed for precise injection of solid feedstock into the reaction zone. Figures 4a,b present a schematic of this mechanism: At the beginning of a test, the solid feedstock is placed in the bottom of the lift tube which is cold enough to keep the feedstock at a safe place and far from the reaction zone so that its composition does not change due to heat. Then, the lift tube is filled with nonfeedstock solid particles up to the middle of the reaction zone. The bed of the nonfeedstock solid particles is fluidized with an inlet gas from the middle of the lift tube and induction heating power supply is switched on to heat up the reaction zone (Figure 4a). Once required reaction temperature is achieved in the reaction zone, direction of the inlet gas is switched to an inlet from the bottom of the lift tube to lift the solid feedstock through the nonfeedstock solid particles toward the reaction zone in less than a second (Figure 4b) by taking advantage of higher superficial gas velocity in the

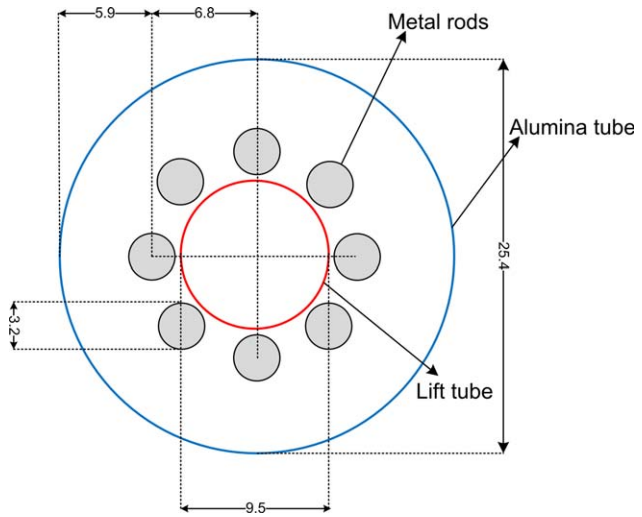

Figure 3. A top view schematic of reaction zone of the IHFBR; dimensions are in millimeter.

[Color figure can be viewed in the online issue, which is available at wileyonlinelibrary.com.]

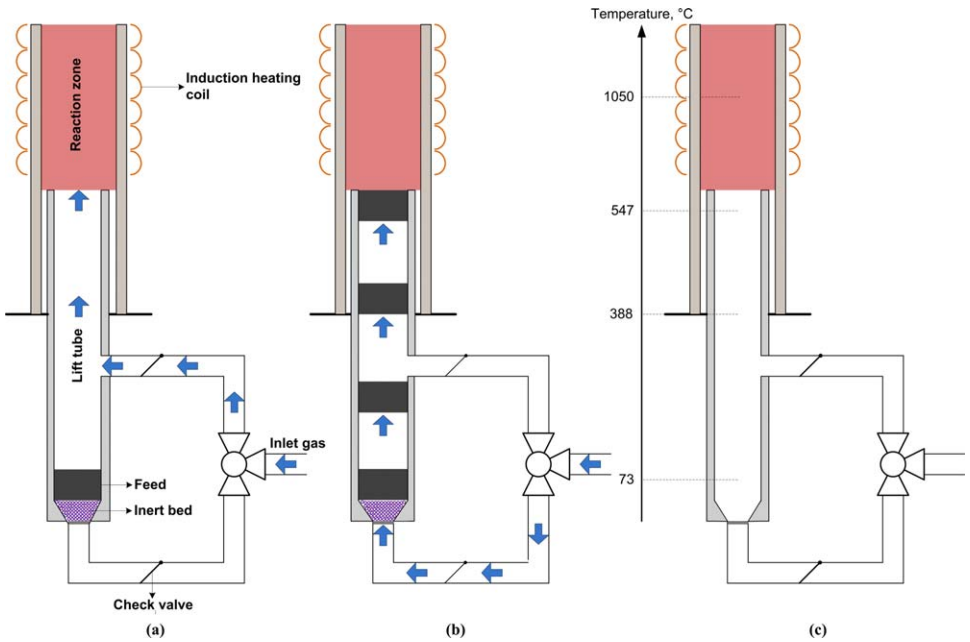

Figure 4. Schematic of the Solid Feed Injection Technique through the Lift Tube; (a) the solid feedstock is stagnant in the bottom while inlet gas enters the lift tube from its middle during heat-up to fluidize the solid particles in the reaction zone; (b) when reaction temperature is reached, inlet gas is switched to the bottom of the lift tube to lift the solid feedstock upward to the reaction zone; (c) An example of temperature profile from bottom of the lift tube to the reaction zone.

[Color figure can be viewed in the online issue, which is available at wileyonlinelibrary.com.]

lift tube than that in the fluidized bed. For instance, when a bed of sand particles with size distribution of 212 to 250 μm is fluidized at temperature 1000°C at $\frac{U}{U_{mf}}$ =2.3, superficial gas velocity in the lift tube and in the fluidized bed was estimated to be 34 and 9 cm/s, respectively.

This mechanism of solid transportation in the lift tube is achieved by segregation between particles of the solid feedstock and the nonfeedstock solid particles. In other words, density and size distribution of the nonfeedstock particles as well as gas velocity (the latter is limited by operation requirements) must be chosen in such a way that the feedstock particles move upward through the nonfeedstock particles in the lift tube and then stay in the fluidized bed of the reaction zone. Fotovat and Chaouki showed how cylindrical particles of biomass (size: 6.4 × 12.7 mm^2; density: 824 kg/m^3) can be either segregated or floated in a bed of sand particles (average diameter: 380 μm; density: 2650 kg/m^3) as a function of gas velocity[20].

Proper placement of the solid feedstock in the bottom of lift tube is very important to lift up all particles of the feedstock. Therefore, as highlighted in Figure 4, internal diameter in the lowest section of the lift tube has a conical geometry in which a bed of nonfeedstock particles is placed on top of a perforated mesh. This bed plays a distributor role and helps the inlet gas to lift whole mass of the feedstock.

Design of the lift tube overcomes two major challenges in solid feeding: storage of a solid feedstock somewhere safe and cold enough so that its composition remains unchanged as well as proper and quick technique for solid injection to the reaction zone at the desired temperature.

One significant feature of the IHFBR is that on the contrary to conventional mini fluidized bed reactors, there is no porous or perforated distributor nor sparger for gas distribution into the fluidized bed. However, as it will be discussed later, the lift tube plays role of the gas distributor.

Storage of the solid feedstock in the lift tube, before injection, is accomplished due to the fact that induction heating is a very fast heating mechanism compared with conventional conduction, convection and radiation heat transfer mechanisms, so the segment of the conductive material which is inside the magnetic field gets heated much faster than the segment outside the magnetic field. Therefore, the segment outside the magnetic field remains cold until conduction heat transfer transfers heat from the hot segment. Figure 4c illustrates an example of temperature profile from bottom of the lift tube to the reaction zone 5 min after temperature was stable at 1050°C in the reaction zone.

Another significant importance of the lift tube is its impact in minimizing the defluidization state in the reaction zone during heat-up process. For instance, when silica sand particles reach the sintering temperature, they get softer and tend to stick together and form agglomerates. Therefore, they must be fluidizing during heat-up to prevent agglomeration.

The alumina tube has to be fixed on a metal flange firmly to avoid gas leakage from the bottom. However, to prevent the metal flange to be heated by induction heating, it is located lower than top of the lift tube. As a result, there is a tiny space between outer wall of the lift tube and internal wall of the alumina tube, which is filled with nonfeedstock particles. This stagnant section does not have any effect on reaction progress.

Depending on application, product gases can be passed through a condenser to collect condensable products and then noncondensable products leave the condenser. In addition, interested product gases can be either collected in a gas-sampling bag or be sent directly toward gas analyzers. MKS multigas Fourier Transform Infra Red (FTIR) and Agilent micro gas chromatography (GC) are used to analyze the product gases. The designed condenser is an aluminum

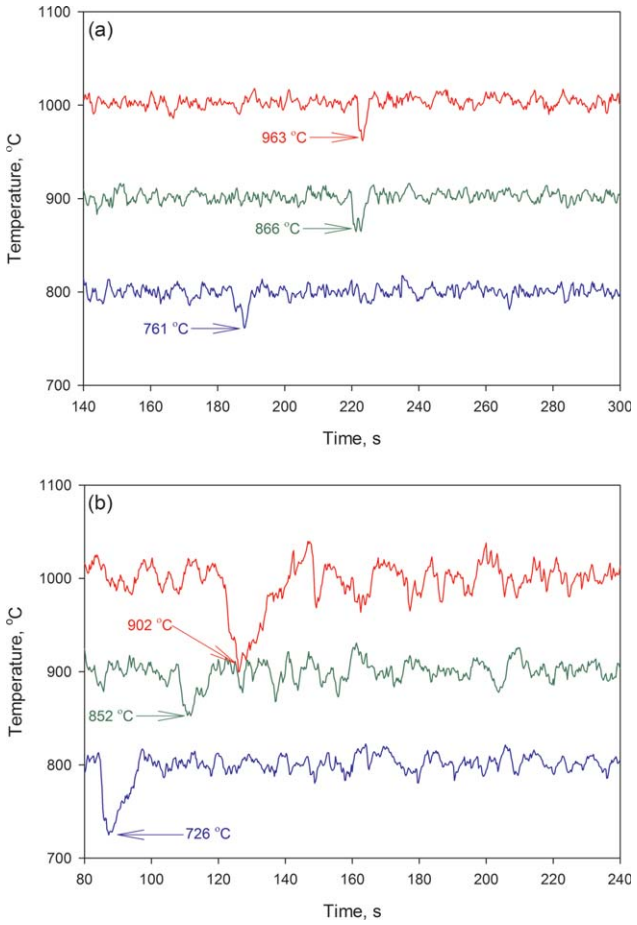

Figure 5. Heating performance of induction heating mechanism in the IHFBR with (a) eight and (b) four stainless steel rods; arrows show the time the feedstock was injected.

[Color figure can be viewed in the online issue, which is available at wileyonlinelibrary.com.]

container with 0.025 m internal diameter and 0.08 m length. Inlet tube of condenser is bent for 45°, so the hot flow of product gases swirls inside the condenser similar to flow inside a cyclone; condensable products are collected in the bottom of condenser and noncondensable gases flow out through the outlet tube. The condenser is placed inside a container containing a mixture of ice and cold water to keep wall temperature of the condenser at 0°C. In cases hot vapors must be sent directly to FTIR to determine the gas composition, the condenser is installed between FTIR and GC.

Performance of the Induction Heating

Pyrolysis of 750 mg of coal with size distribution of 212–250 μm in a fluidized inventory of 50 g silica sand with similar size distribution was conducted to evaluate performance of the induction heating at temperatures 800, 900, and 1000°C. Figure 5a presents the time at which coal was injected, the following temperature drop of the bed and response of the induction heating. Eight stainless steel rods were used as the heating elements. Although 35–40°C temperature drops were observed, it took only 3–5 s for the bed to return to the setpoint temperature. This observation of fast response reveals robust performance of the induction heating to supply the required heat.

It is important to note that number of the metal heating elements has significant impact on performance of the induction heating. To study effect of this parameter, coal pyrolysis tests with four stainless steel rods were carried out (Figure 5b) under operating conditions similar to those associated with Figure 5a. As presented in Figure 5b, cutting off number of the heating metal rods by half not only caused temperature drops of 50–100°C, but also it caused temperature recoveries to take between 15 and 20 s. This observation was simply because there were less metal rods to absorb energy of the magnetic field and as a consequence there was less heating source.

In fact, the associated energy of the magnetic field, which is generated by induction heating, is partly consumed by the cooling water flowing through the coil, and the metal rods in the fluidized bed absorb the remaining.

After estimations of the total power supplied by the induction heating power supply and estimation of the power consumed by cooling water, it was revealed that the metal rods (eight rods) absorb a net 6.4 kW power after the initial power is delivered to the coil to compensate temperature drop on injection of the feedstock. This power is, in turn, transferred to the bed through radiation and convection heat transfer. This amount of heat is huge in comparison with conventional external heaters that are used to heat up similar inventories in a fluidized bed. Maximum power supply by an external heater is about 2.5 kW.

Regardless of the power quantity, induction heating is a very fast response system in term of delivering the required power. Response time of the temperature controller is 85 ms. Furthermore, the used induction heating mechanism is internal and all heat is consumed in the bed in contrary to the cases with external heaters from which a large portion of the radiated heat heats up mass of the reactor tube located inside the furnace and a large portion is lost to environment. It has been observed that it would take 3–5 min to recover 50°C temperature drop by the external furnaces.

It is noteworthy that initial heating-up and postreaction cooling-down steps are also very fast by induction heating. For instance, it takes 45 s for the IHFBR to reach 1000°C from room temperature while it takes 2 h by a 2.3 kW external furnace. This feature significantly help save time in favor of performing many tests, that is, one complete test per half an hour.

Feedstock Temperature Inside the Lift Tube

It was mentioned earlier that the lift tube facilitates preserving the feedstock away from the reaction zone until the setpoint reaction temperature is achieved (Figure 4). Besides, it is significantly important that the feedstock does not undergo prethermal cracking before getting into the reaction zone while travelling through the lift tube.

Assuming all the heat is transferred to the feedstock along the lift tube, temperature increase in mass of the feedstock, T_f, can be expressed as

$$m_f C_{P,f} \frac{dT_f}{dt} = hA(T_l - T_f) \tag{2}$$

Setting a $= \frac{hA}{m_f C_{P,f}}$, integration of Eq. 2 results in

$$T_f = T_l - (T_l - T_{f,0}) \exp(-a\Delta t) \tag{3}$$

Temperature profile in the lift tube vs its length had a trend of $T_l = 180.2 \ln(x_l) + 75$ according to data in Figure 4c;

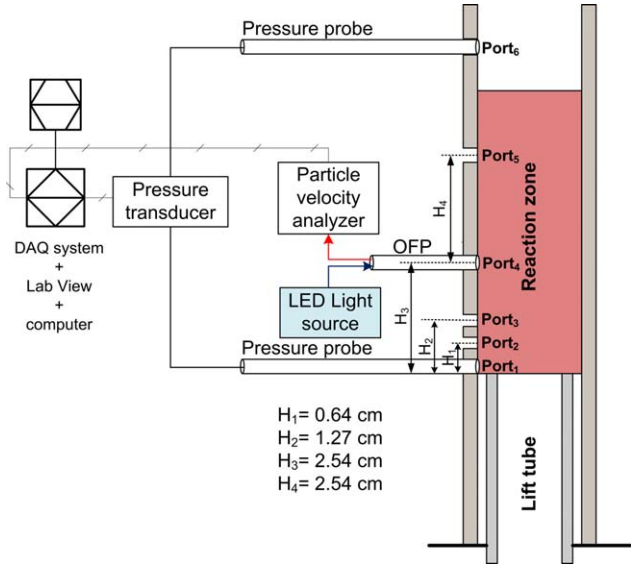

Figure 6. A schematic of the setup for fluidization quality studies in the IHFBR; presented layout of the probes is an example only.

[Color figure can be viewed in the online issue, which is available at wileyonlinelibrary.com.]

integrating this equation, an average lift tube temperature of 400°C was considered. Then, estimations showed that the lifting time, Δt, for a 750 mg mass of coal was about 0.7 s and heat transfer coefficient[21] was 76 W/m^2 K in the 15 cm long lift tube. As a result, it was estimated that temperature of coal would be 126°C at the time of entering the reaction zone which is fluidized at 1050°C. Such a temperature increase is too low to cause any significant thermal decomposition on the feedstock.

It is noteworthy that the temperature profile presented in Figure 4c was obtained after 5 min of operation whereas, in practice, the feedstock is injected shortly after the reaction temperature is achieved; in such consequences, temperature profile in the lift tube is much milder and the feedstock is preserved at a lower temperature. In addition, zero heat loss to sand particles and environment was assumed in Eq. 2. Thus, the lift tube is proved to be providing a very efficient feeding technique for direct introduction of the feedstock to the reaction zone similar to that in industrial fluidized bed reactors.

Fluidization Quality in the IHFBR

As highlighted earlier, the lift tube plays role of a gas distributor in the IHFBR; therefore, it is important to study whether quality of fluidization is similar to that in the conventional fluidized bed reactors and how bubbles are formed on top of the lift tube.

To do so, a transparent acrylic tube with dimensions similar to those of the alumina tube was used with measurement ports 1–5 along the fluidized bed of the reaction zone and measurement port 6 located above the fluidized bed. A differential pressure transducer was used to measure bed expansion and bed voidage in the segments of the reaction zone between two ports. An optical fiber probe (OFP) was in addition used to measure local bed voidage at different axial and radial locations in the fluidized bed. Different configurations were used by changing location of the OFP and probes of the pressure transducer. Figure 6 depicts one configuration of the measurement probes on the setup.

Fluidization studies were carried out at room temperature while the heating rods were available inside the reactor. However, due to diameter of the OFP, one rod was taken off in order for the probe to face the fluidized bed.

The OFP contained 72 emitting and receiving plastic fiber strands with 250 μm diameter arranged in an alternative array; the bundle of the fibers was placed in a tube with 3 and 4.7 mm internal and external diameters, respectively.[22,23] An LED light source with light intensity set at 360 supplied the required light. The outlet of receiving fibers was connected to a PV-4A particle velocity analyzer in which variation of the received light vs time corresponding to real-time local bed voidage could be obtained in the form of variation of voltage vs time. Voltage signals had to be tuned to vary between two extremes corresponding to the empty reactor (zero solid concentration) and the minimum fluidization state. Sampling rate of the acquired voltage signals was adjusted at 400 kHz. Equations 3 and 5, developed by Cui et al.,[24,25] were used to convert real-time local voltage signals (local voltage vs time), from the OFP, to real-time local bed voidage signals, that is, $\varepsilon_{r,loc}$ vs time

$$\frac{1-\varepsilon_{r,loc}}{1-\varepsilon_{mf}}=\frac{0.4u}{1.4-u} \tag{4}$$

where

$$u=\frac{V-V_0}{V_{mf}-V_0} \tag{5}$$

V_{mf} and V_0 are two voltage extremes corresponding to minimum fluidization state and an empty bed, respectively, that are set by calibration. V is the real-time local voltage that varies between V_{mf} and V_0 when the bed is fluidized. Figures 7a–c in the later section present some examples of real-time local bed voidage signal.

Equation 6 was used to estimate bed voidage (ε) associated with a bed segment. Pressure drop (ΔP) in Eq. 6 was equal to average of recorded real-time pressure drop fluctuations between two ports of the pressure transducer

$$\frac{\Delta P}{\Delta H}=\rho_p(1-\varepsilon)+\rho_g\varepsilon \tag{6}$$

Fluidization dynamics experiments were carried out with silica sand of 212–250 μm size distribution, representing Geldart's group B powders, and with FCC catalyst particles of 70–90 μm size distribution, representing Geldart's group A powders.

Fluidization Dynamics in the IHFBR

Having said that internal diameter of the reaction zone was 2.54 cm, it was understood from the visual investigations that in case of the Geldart's group B particles when superficial gas velocity was three times as much as minimum fluidization velocity, large bubbles produced slugging conditions in the reactor, so mixing quality was poor. In addition, high gas velocities would result in solid entrainment. Therefore, the IHFBR operates at $\frac{U}{U_{mf}}$ ratios below 3 for the Geldart's group B particles. In case of the Geldart's group A particles, no slugging was observed at tested $\frac{U}{U_{mf}}$ ratios up to 7, but solid entrainment was badly observed.

Figures 7a–c depict some real-time local bed voidage signals in center of the reactor and at different heights, from the top of the lift tube. Also, Figure 7d presents real-time

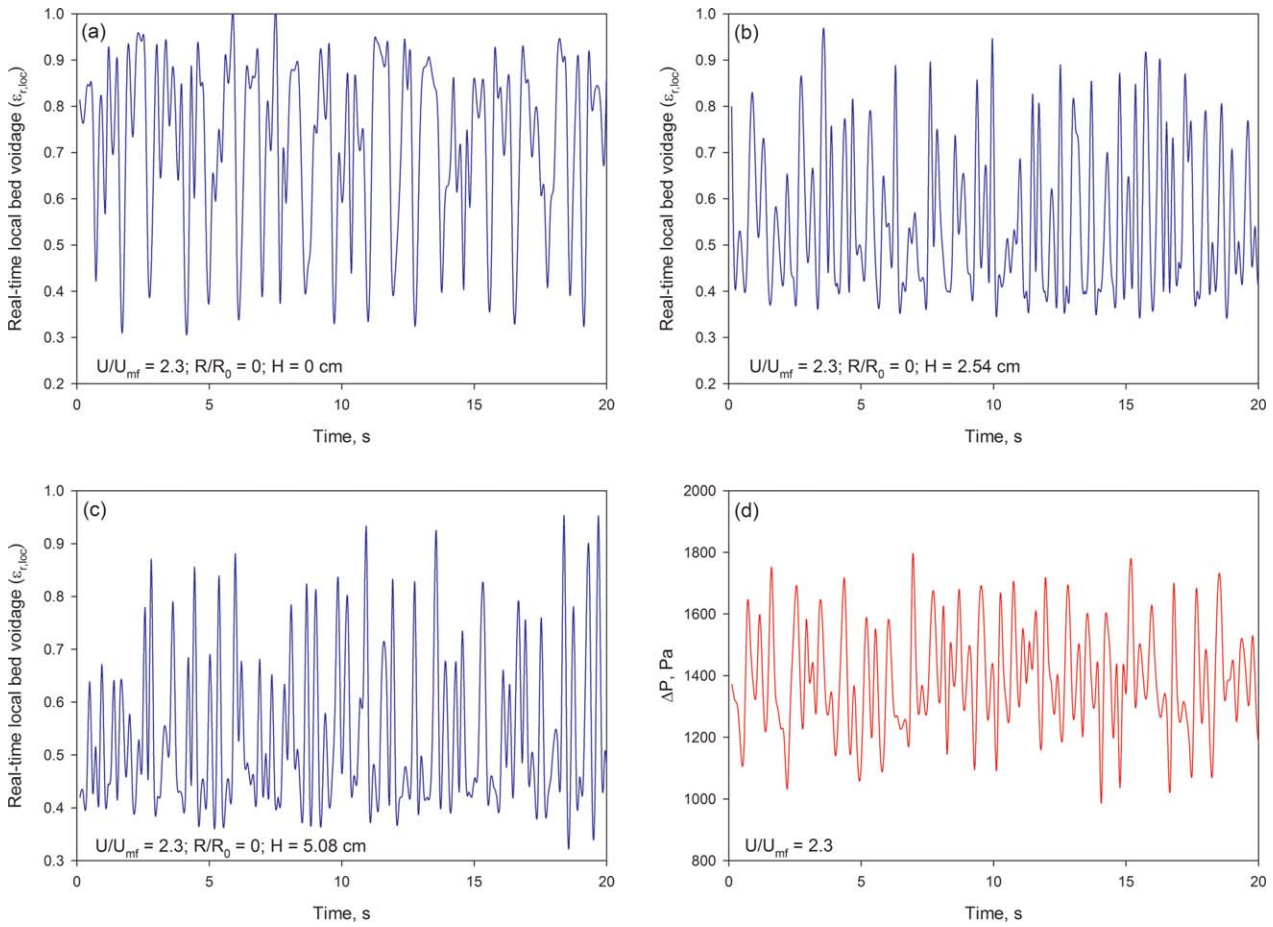

Figure 7. Bed voidage and pressure drop fluctuations of sand particles in the reaction zone of the IHFBR: (a), (b), and (c) local measurements by the optical fiber probe; (d) pressure drop measurements of the whole bed.

[Color figure can be viewed in the online issue, which is available at wileyonlinelibrary.com.]

pressure drop fluctuations of the whole bed of sand particles in the reaction zone of the IHFBR.

Such fluctuations in Figure 7 are true indications that particles were well fluidized in the reaction zone of the IHFBR as they are similar to the wavy fluctuations in the conventional fluidized bed reactors. These fluctuations also indicate occurrence of gas-solid mixing and coalescence and breakage of the bubbles continuously in the IHFBR. It will be discussed later that such fluctuations were not observed through OFP measurements on the wall in opposite to the tip of the lift tube.

Investigation of the Bed Voidage in the IHFBR

To verify uniform bed voidage in the fluidized bed of the IHFBR, average value of the pressure drop fluctuations associated with a segments of the bed, that is, bed between two ports of the pressure transducer, was used; then, the corresponding bed voidage was estimated using Eq. 6. Time span of the used pressure drop fluctuations was 30 s. As seen in Tables 2 and 3, estimated bed voidage values at a given $\frac{U}{U_{mf}}$ were found almost similar at different segments for the sand and the FCC particles.

To confirm reliability of such results, average of the estimated bed voidages at a given $\frac{U}{U_{mf}}$ was used to calculate average total bed height of the fluidized bed. The obtained results, presented in Tables 2 and 3, were in very good agreement with visual observations of the total bed heights.

To study how bubbles are formed on the top of the lift tube and how their evolution patterns are followed in the reaction zone, local bed voidage (ε_{loc}), average value of the recorded real-time local bed voidage at the associated local $(\varepsilon_{r,loc})$, was used. Beforehand, the OFP was placed at different radial and axial locations in the reaction zone; then, Eqs. 3 and 5 were used to obtain real-time local bed voidages over 30 s time span.

The local bed voidages in the fluidized beds of sand and FCC particles are presented in Figures 8 and 9, respectively, for different superficial gas velocities in the reaction zone. A similar axial evolution of the local bed voidage from the top of the lift tube toward surface of the fluidized bed was obtained in all cases. In other words, gas concentration at the tip of the lift tube, where $\frac{R}{R_0}=0$ and 0.5, was high which implies formation of large bubbles in that spot. Such large bubbles were formed due to the fact that internal diameter of the lift tube was smaller than internal diameter of the reaction zone, so gas velocity was accordingly larger just before exiting the lift tube. For instance, when gas velocity in the bed of sand particles was 10 cm/s, it was 70 cm/s at the exit of the lift tube. Since gas velocity was reduced at the exit of the lift tube, its associated kinetic energy declined accordingly, and as a result, breakage of the large bubbles occurred

Table 2. Bed Voidage and Bed Height Estimations of Sand Particles in the Reaction Zone from Pressure Drop Measurements

Bed segment on the top of lift tube	$\frac{U}{U_{mf}}=2.3$	$\frac{U}{U_{mf}}=2.1$	$\frac{U}{U_{mf}}=1.9$
Lift tube–port 4	0.52	0.52	0.52
Port 4–port 5	0.48	0.48	0.49
Lift tube–port 5	0.50	0.50	0.50
Total bed height, cm	10.8	10.4	10.0

which were distributed across the bed consequently. Interestingly, it is seen in Figures 8 and 9 that there was uniform local bed voidage distribution at axial distances farther than 1 cm of tip of the lift tube.

Regardless of axial bubble formation-breakage phenomenon caused by the lift tube, local bed voidage on the wall of the reaction zone was less than neighboring internal radial locals at a given height. This should indicate that concentration of emulsion phase was higher on the wall while bubble phase was dominant in the internal radial locals. Then, it can be concluded that there was a mixing pattern in the reaction zone of the IHFBR similar to mixing conditions in the conventional fluidized bed reactors.

It is important to specify if there is any defluidized spot in the bed, in particular near the wall, due to gas distribution from the lift tube. It is seen in Figures 8 and 9 that despite the cases for $\frac{R}{R_0}=0$ and 0.5, local bed voidage on the wall, $\frac{R}{R_0}=1$, has an increasing trend starting from the point that is in front of the lift tube ($\frac{R}{R_0}=1$ and $\Delta H=0$) until it reaches a stable local bed voidage at farther axial distances. In fact, despite the wavy fluctuations of OFP data shown in Figure 7, the OFP signal associate with locals on the wall in front of the lift tube ($\frac{R}{R_0}=1$ and $\Delta H=0$) was almost a straight line. This observation indicates that zone was actually a defluidized zone; such result was expected because when a bubble is formed at the tip of the lift tube, its diameter cannot be larger than internal diameter of the lift tube. Conversely, the OFP signals related to the axial locals on the wall and above the tip of the lift tube ($\frac{R}{R_0}=1$ and $\Delta H>0$) presented a fluctuating pattern indicating presence of bubbles formation and breakage, and therefore, proving such zones were not defluidized.

According to Figures 8 and 9, the defluidized zone on the wall was until a height below 0.8 cm distance from the tip of the lift tube, but it was not possible to find the exact height by the OFP measurement technique due to limitations caused by dimensions of the reactor. In spite of this, with respect to the estimated local bed voidage data for sand particles at $\frac{R}{R_0}=0,\ 0.5$, and 1 within this distance, it was interpolated that the local bed voidage would be about 0.47 at a 1×10^{-3} m distance from the wall; therefore, it was realized that the volume of defluidization zone was almost negligible.

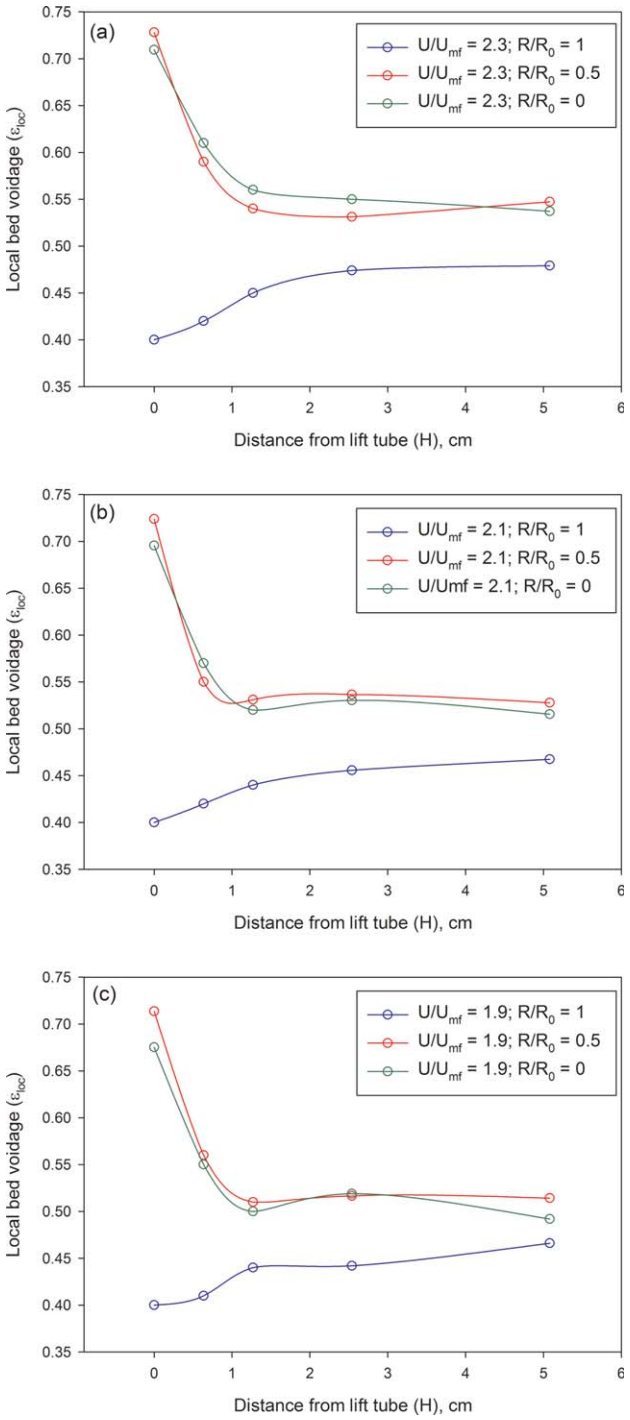

Figure 8. Axial and radial bed voidage evolution in a bed of sand particles in the reaction zone of the IHFBR.

[Color figure can be viewed in the online issue, which is available at wileyonlinelibrary.com.]

Table 3. Bed Voidage and Bed Height Estimations of FCC Particles in the Reaction Zone from Pressure Drop Measurements

Bed segment on the top of lift tube	$\frac{U}{U_{mf}}=8$	$\frac{U}{U_{mf}}=6.7$	$\frac{U}{U_{mf}}=5.3$
Lift tube–port 4	0.65	0.65	0.67
Port 4–port 5	0.67	0.67	0.66
Lift tube–port 5	0.66	0.66	0.67
Total bed height, cm	11.1	10.7	10.5

Influence of Lift Tube on Bed Expansion

As illustrated in Figure 2, the reaction zone and the lift tube are both filled up with the nonfeedstock particles during preparation of the setup. It has been observed that after the solid particles start to fluidize in the reaction zone, some

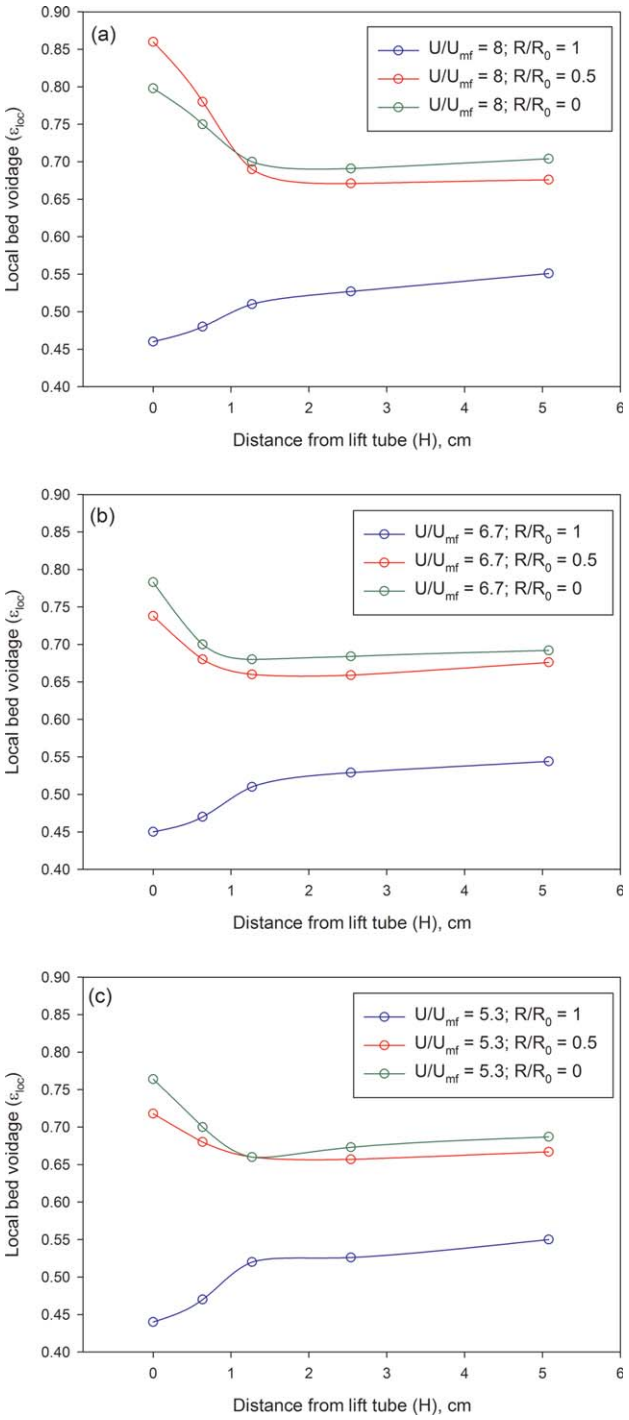

Figure 9. Axial and radial bed voidage evolution in a bed of FCC particles in the reaction zone of the IHFBR.

[Color figure can be viewed in the online issue, which is available at wileyonlinelibrary.com.]

particles enter the reaction zone from the lift tube and influence the bed expansion. Thus, it is important to understand how much this contribution is to the total bed height of the reaction zone.

To investigate this occurrence, two series of experiments with silica sand and FCC catalyst particles were carried out where pressure drop of the bed between ports 1 and 6 in Figure 6 was estimated vs superficial air velocity.

Figure 10 illustrates variations of $\frac{\Delta P}{\Delta P_{max}}$ vs superficial air velocity and ratio of $\frac{U}{U_{mf}}$ for both sand and FCC particles. Maximum pressure drop was estimated according to initial mass of the particles in the reaction zone at fixed bed condition.

Having said that estimated minimum fluidization of the used sand particles was 4.4 cm/s, it is seen in Figure 10a that when minimum fluidization state was reached, $\frac{\Delta P}{\Delta P_{max}}$ ratio was 1.86 that is in contrary to the expected value of unity in a conventional fluidized bed reactor. In other words, estimations showed that 43% of mass of sand in the lift tube was added to the reaction zone at minimum fluidization condition. From another point of view, the $\frac{\Delta P}{\Delta P_{max}}$ ratio was around unity when $\frac{U}{U_{mf}}$ was about 0.6 implying contribution of solids in the lift tube to the bed expansion even before minimum fluidization state. Interestingly, sand particles kept entering the reaction zone at superficial air velocities above U_{mf}. Similar trend was observed with FCC catalyst particles as shown in Figure 10b for superficial air velocities around and above U_{mf}.

It is realized from such results that when the reaction zone is well fluidized, there is a diluter concentration of solids in

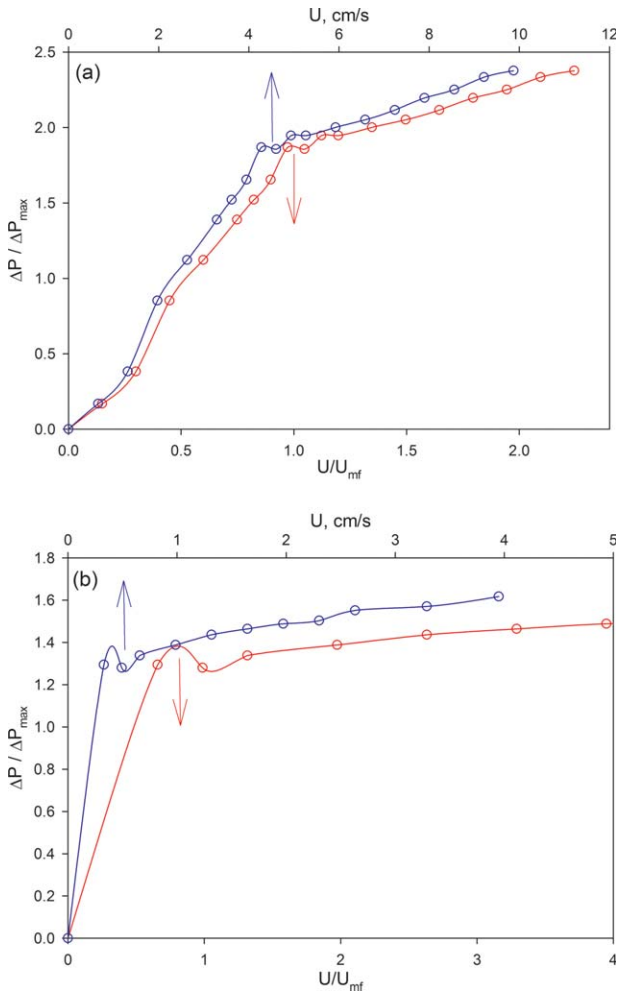

Figure 10. Influence of the lift tube on bed expansion in the reaction zone of the IHFBR (a) sand (b) FCC; blue color presents *U* and red color presents $\frac{U}{U_{mf}}$.

[Color figure can be viewed in the online issue, which is available at wileyonlinelibrary.com.]

the lift tube that helps it to have a better performance when inlet gas is switched to bottom of the lift tube to lift the feedstock toward the reaction zone. If there was a very dense concentration of the nonfeedstock solids in the lift tube, upward movement, and segregation of the feedstock particles would have been very poor due to insufficient moving space.

High Temperature Screening Tests

Operating conditions of the IHFBR

Superficial Gas Velocity. The IHFBR operates at bubbling regime. Figure 10 presents superficial gas velocities corresponding to each $\frac{U}{U_{mf}}$ during operation at room temperature with either sand (212–250 μm) or FCC particles.

Having flow rate of the inlet fluidizing gas fixed, it has been observed that intensity of particles mixing is promoted at higher temperatures. In other words, minimum fluidization velocity decreases vs an increase in temperature. Therefore, in case it is required to maintain a bubbling bed with similar intensity of fluidization, for instance $\frac{U}{U_{mf}}=2.5$, at any temperature, flow rate of the inlet gas should decrease accordingly. Pressure drop measurements with a differential pressure transducer showed that minimum fluidization velocity of the bed of sand with size distribution of 212–250 μm was reduced by a factor of $(U_0+0.6)\frac{T_0}{T_{bed}}$ up to temperature at 1000°C. According to the discussion in the preceding section, minimum fluidization velocity was found when $\frac{\Delta P}{\Delta P_{max}}$ was 1.86. Pressure drop measurements were carried out while the rods were kept in the fluidized bed.

Temperature. Design of the reactor (high temperature resistance of the alumina tube and the heating element rods) provides potential of operation until 1500°C. In case extremely high temperature reactions (1200–1500°C) should be investigated while catalytic effect is not a concern, such as in a combustion environment, platinum rods made of a platinum alloy, 90% platinum, and 10% iridium are used. In other cases in which platinum has catalytic effect such as pyrolysis and gasification reactions, metal rods made of Inconel or stainless steel can be used.

Particles Size and Type. The IHFBR can be fluidized with nonfeedstock solid particles such as inert sand, olivine, and catalyst particles with size distributions up to 350 μm; this limitation is governed by geometry of the reactor. The IHFBR was designed for screening tests of reactions containing solid reactants with a wide range of high temperatures. To do so, depending on the application, type and particle-size distribution of the nonfeedstock solid particles of the fluidized bed must be well chosen. For instance, a bed of sand particles with size distributions of 105–212 μm was completely defluidized in the reactor at 800°C in the absence of any reaction, but there was no defluidization state when sand particles with size distribution of 212–250 μm was used. As another example, the latter was defluidized at 1100°C, but when alumina particles with similar size distributions were used, defluidization state was not observed at similar $\frac{U}{U_{mf}}$ condition.

These defluidization observations indicate significant presence of the interparticles forces which govern quality of fluidization at high temperatures. In such cases, inter particle forces were even stronger than hydrodynamics forces,[22,23] and the defluidization state occurred because solid particles reached the sintering temperature and became soft. As a matter of the fact, sintering temperature of the solids is 0.4–0.9 times as much as their melting temperature. Sintering temperature of the solids with smaller size distributions is lower than that of similar solids with larger size distributions.[26–29]

Back-Mixing of Feedstock Particles. During early stage development of the reactor, back-mixing of the feedstock particles was a concern, so it was well checked with several tests of coal combustion: after a test, the particles in the reaction zone were removed; then solids remaining in the lift tube were examined and no trace of coal particles, that is, no back-mixing was observed. This could be due to the following reasons:

When solid feedstock is injected to the bed, reaction takes place and particles instantly become smaller, so their tendency to stay in bed is highly increased. Furthermore, diameter of the lift tube is almost 2.7 times smaller than diameter of the fluidized bed, and consequently, gas velocity at the exit of the lift tube is 7.3 times larger. These two effects help keep solid feedstock in the fluidized bed.

In situ emissions reduction in coal fired boilers

Coal combustion is the most common heat supply process for electricity generation in the power plants in countries such as the United States and China. Conversely, there are serious environmental problems associated with the emissions from such coal fired boilers: since coal contains elements such as sulphur, nitrogen, and mercury, they are released to atmosphere in different forms that are definitely detrimental to environment and humans' life. For instance, release of gases such as SO_2, SO_3, NO, and NO_2 leads in formation of acidic rains as a result of contact with humidity. Concentration of these emissions in the outlet of coal fired boilers is usually larger than the permitted limits. As an example, concentration of SO_2 and NO_2 from coal combustors before gas cleaning is 200–2000 and 800 ppm, respectively.[30]

In some countries, there are legislations to control concentration of emissions and to keep it below the standard levels. For example, according to the National Ambient Air Quality Standards (NAAQS) set by the Environmental Protection Agency (EPA) in the US, concentration of the released SO_2 and NO_2 must be below 100 and 75 ppb, respectively.[31]

As a matter of the fact, there are 557 power plants in the Units States as of 2010[32] that must take the EPA standards into account. Although there are gas-cleaning technologies such as scrubbing and absorption, installation and operation of such technologies will impose huge capital and utility costs to these existing power plants.

In situ emissions reduction is an alternative to minimize or cutoff release of such toxic gases to atmosphere through addition of economical alkali (Na or K) or earth alkali (Ca) bearing sorbents to coal before feeding into the combustor.[33–35] For example, if $Ca(OH)_2$ was mixed with coal, it would decompose at high temperatures to CaO and H_2O; then CaO would react with SO_2 and SO_3 according to reactions 1 and 2 inside the boiler to form solid CaS (malting point: 2525°C) and $Ca(SO)_4$ (melting point: 1460°C) that would be precipitated in the downstream separation steps after the boiler

$$CaO+SO_2 \rightarrow CaS(s)+\frac{3}{2}O_2 \qquad \text{(Reaction 1)}$$

$$CaO+SO_3 \rightarrow Ca(SO_4)(s) \qquad \text{(Reaction 2)}$$

Likewise, if Na_2CO_3 was mixed with coal, SO_2 would be captured according to Reaction 3

$$Na_2CO_3 + SO_2 + \frac{1}{2}O_2 \rightarrow Na_2SO_4(s) + CO_2 \qquad \text{(Reaction 3)}$$

To enhance impact of the in situ emissions reduction method, a ReEngineered Feedstock™ (ReEF™) composed of combustible components of municipal waste such as hard plastic, soft plastic, and fiber including a sorbent has been developed by the Accordant Energy™.[36,37] Since nitrogen and sulphur content of ReEF™ is very low and almost negligible, this feedstock is designed to be cofired with coal to decrease coal consumption in favor of reduction of NO_x and SO_x emissions. Also, since ReEF™ contains chlorine, mercury content of coal can be captured in the form of mercury chloride.

Despite promising features of the coal + sorbent combustion and coal cofiring with feedstocks such as ReEF™, the process must be optimized with the most suitable sorbent, ReEF™ formulation and mass ratio between coal, sorbent and reEF™ so that the desired level of emissions can be achieved. From another perspective, coal fired boilers are classified as fluidized bed coal fired boilers and pulverized coal fired boilers; each of these combustors should operate at different temperatures with different particle-size distribution of coal, sorbent and ReEF™. Therefore, there is a large array of screening tests to investigate an optimized operating condition for the in situ emissions reduction for either coal fired boiler. Conversely, utilization of a large scale setup to be used as a pulverized or fluidized bed coal fired boiler to carry out such screening tests is definitely costly, time taking, and labor demanding.

Another critical challenge in utilization of sorbents in coal firing, in particular, in fluidized beds is occurrence of the defluidization state when an alkali bearing sorbent is used that will be discussed in a later section. In opposite, interestingly, higher emissions reduction is achieved when an alkali bearing sorbent is used in comparison with influence of an earth alkali bearing sorbent. Therefore, prediction of the defluidization state must be taken into account to find process operating conditions at which the defluidization state does not happen at the presence of an alkali bearing sorbent. Occurrence of the defluidization state in a large scale fluidized bed causes a lot of operation delays due to overhaul, reactor cleaning, and bed material loading.

Fast heating rate, quick and accurate solid feeding technique, its durability at extremely high temperatures and its convenient and rapid operation make the IHFBR overcome atop mentioned challenges in screening tests for in situ emissions reduction during coal combustion or coal cocombustion. In addition, as it will be discussed in a later section, this novel reactor is an ideal setup to predict the defluidization state very quickly. Therefore, the IHFBR facilitates performing a large set of screening tests while considerable amount of time and cost, that is, cost of material, operation, and equipment, can be saved.

In Situ SO_x Reduction Tests in the IHFBR

Representative experimental data of coal + sorbent combustion tests is presented to illustrate performance of the IHFBR to detect influence of a sorbent in SO_x reduction, and to explain the applied feed preparation technique that led to generation of reproducible data.

A sample of coal, containing 1.3 wt % sulphur, was prepared with particle-size distribution of 212–250 μm. Runs were carried out with coal and mixtures of coal + sorbent. Mass ratio of sorbent and coal were adjusted so that alkali or earth alkali to sulphur molar ratio, with general ratio formula of $\frac{Ca+Na/2}{S}$, varied among 1, 2, and 3. Since mineral sorbents included very fine particles (15 μm average size), true feeding of whole mixture of coal and sorbent was not possible through the lift tube. Therefore, the following procedure was followed to coat sorbent powders on coal particles:

- Sorbent was dissolved in de-ionized water;
- The solution was added to coal;
- The resulting slurry was placed in oven over the night at 105°C;
- Dried residue was gently crushed.

To do a test, a 750 mg mass of coal or mixture of coal and sorbent was placed in the bottom of the lift tube and then the reactor was filled up with sand of 212–250 μm size distribution. The Reaction zone of the IHFBR was fluidized with air from middle of the lift tube until temperature reached 900°C. Then, air was switched to oxygen and then the inlet gas was switched to the bottom of the lift tube to lift the feedstock to the reaction zone. The MKS multigas FTIR analyzed the product gases, which were collected in a gas-sampling bag within 90 s. Each run was repeated for three times to test reproducibility of data.

A typical FTIR acquisition signal from a gas-sampling bag is presented in Figure 11 where production of CO_2, SO_2, and SO_3 is compared in the absence and in the presence of a calcium bearing sorbent X_1 $\left(\frac{Ca+Na/2}{S}=3\right)$. It should be noted that product gases collected in the bag were sucked toward FTIR by a low vacuum pressure until a well representative concentration, that is, stable concentration of the gases was acquired.

It is realized from Figure 11 that a significant reduction in SO_x generation was obtained when sorbent X_1 was added to coal particles while production of CO_2, main combustion product gas, was similar. Given the fact that sorbent X_1 was adhered to coal and it was not added at a level before which SO_x was generated, such result indicate that Reactions 1 and 2 occurred instantaneously to convert SO_x to solids.

Reduction in SO_2 and SO_3 vs $\frac{Ca+Na/2}{S}$ ratios obtained from coal combustion at 900°C assisted with sorbents X_1, X_2, and mixture of sorbents X_2 and X_3 is presented in Table 4. Sorbents X_1 and X_2 contained calcium while sorbent X_3 contained sodium. The reported reduction yields are associated with difference between generation of SO_x when coal was fed in the absence of any sorbent and generation of SO_x when a mixture of coal and sorbent was fed. The data are average values obtained from three consecutive experiments at similar conditions.

Results prove that addition of sorbents containing alkali and earth alkali elements was very effective to lower generation of SO_x. Larger $\frac{Ca+Na/2}{S}$ ratio resulted in higher reduction in SO_x. Both sorbents X_1 and X_2 contained calcium hydroxide, but sorbent X_1 demonstrated more promising effects. This difference should be related to different molecular structure of the sorbents, which would come into affect when the mineral underwent thermal decomposition.

According to data of sorbents X_2 and X_3 in Table 4, sodium was more effective than calcium in SO_x reduction particularly at lower $\frac{Ca+Na/2}{S}$ ratios.

Low values of the standard deviation data in Table 4 indicate reliable performance of the IHFBR to generate

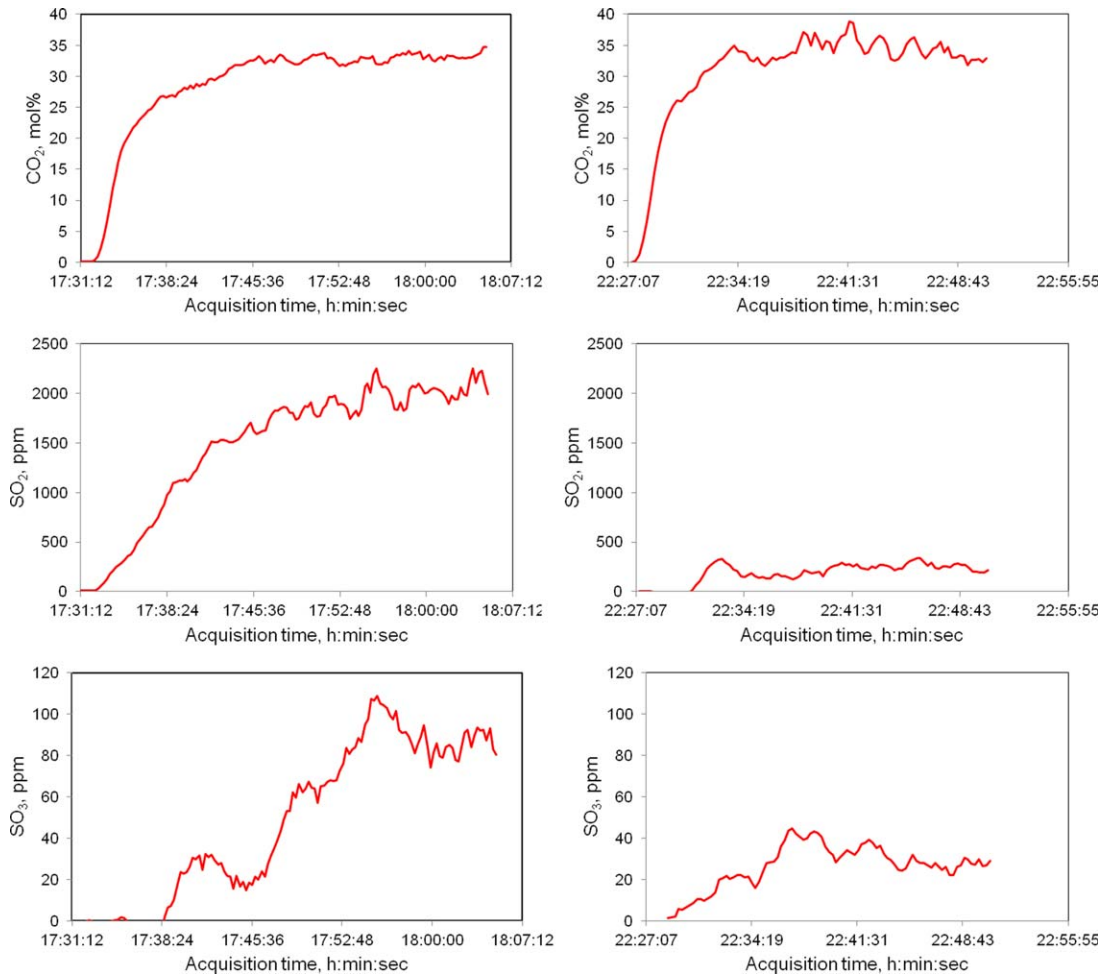

Figure 11. Effect of calcium bearing sorbent X_1 in SO_2 and SO_3 reduction; Left: FTIR acquisition signal in absence of sorbent; Right: FTIR acquisition signal in presence of sorbent X_1 $\left(\frac{Ca+Na/2}{S}=3\right)$; Temperature 900°C.

[Color figure can be viewed in the online issue, which is available at wileyonlinelibrary.com.]

reproducible results. It is also realized that the applied technique to adhere fine powders of sorbents to coal was reasonably efficient.

Defluidization prediction by IHFBR

There are several phenomena that cause the defluidization state to occur in a fluidized bed reactor. As discussed before, one important phenomenon is sintering temperature of the nonfeedstock particles.

It has been reported that in the fluidized bed reactors where a solid fuel such as biomass or coal was fed to a gasification or combustion reactor, the defluidization state occurred in the reactor although the nonfeedstock particles were far from their sintering temperature.[38–49] This phenomenon is due to either the inorganic content of the feedstock which under normal operating conditions can accumulate as a sticky layer that coats the bed material (coating-induced agglomeration) or the alkali components (containing either Na or K) of the feedstock that combine with the bed material forming low temperature melting eutectics at the surface (melt-induced agglomeration). For instance, when there is a sodium bearing component in the feedstock in a bed of silica sand at typical gasification or combustion temperature, silica can react with sodium and form the low-melting silicate $Na_2O{\cdot}3SiO_2$ on the surface of the silica sand particles.

In both cases of coating-induced and melt-induced agglomeration, the nonfeedstock particles tend to stick together and form agglomerates that progressively grow to the point where they lose their fluidizability.

Table 4. Reduction in Production of SO_2 and SO_3 due to Presence of Sorbents X_1, X_2 and X_3 in Coal Combustion; Standard Deviations are Reported in Parentheses

	Coal + sorbent X_1		Coal + sorbent X_2		Coal + sorbents X_2+X_3	
$\frac{Ca+Na/2}{S}$	SO_2 reduction, %	SO_3 reduction, %	SO_2 reduction, %	SO_3 reduction, %	SO_2 reduction, %	SO_3 reduction, %
1	80 (2.2)	48 (0.3)	63 (4.9)	59 (0.5)	85 (1.2)	73 (0.7)
2	89 (5.7)	89 (0.4)	87 (4.2)	70 (0.7)	87 (1.7)	82 (0.3)
3	96 (2.4)	86 (0.8)	91 (0.5)	83 (0.4)	92 (3.3)	97 (0.4)

Figure 12. Agglomerated sand particles in the reaction zone of the IHFBR after combustion of coal with a sodium bearing sorbent.

[Color figure can be viewed in the online issue, which is available at wileyonlinelibrary.com.]

To control and avoid occurrence of the defluidization state, it is crucial to predict agglomeration in the fluidized bed reactors to develop a map or range of operating conditions far from the defluidization state. Important operating conditions in this sort of map could be temperature, gas velocity, mass ratio between coal and alkali bearing sorbent and particle-size distribution of materials. As discussed earlier, development of such a map in a large scale fluidized bed reactor would be time, energy, and labor demanding.

It has been discovered that the IHFBR is an ideal system to detect the defluidization state; therefore, it facilitates investigation of formerly discussed map of operation conditions in terms of time, cost, and labor. An example of the defluidized state in the IHFBR is shown in Figure 12 where a mass of coal coated with sodium bearing sorbent had been fed to a fluidized bed of silica sand particles at 900°C.

It is worth mentioning that in the tests where samples of coal and coal coated with calcium bearing sorbents were fed to a bed of sand particles in the IHFBR, in opposite to the case of sodium bearing sorbents, no defluidization was observed during the operation at 900°C, and as expected, the nonfeedstock particles did not tend to stick to the internal rods which is an indication that rods were not much hotter than the bed. These observations were in good agreement with the report by Latifi et al.[3] that in the fluidized beds where there were internal heating rods, radial temperature profile (between internal rods and sand particles) was very low.

Identification of the defluidization state is achieved in the IHFBR by monitoring temperature profile in its reaction zone: since temperature is supposed to be uniform in the fluidized bed, temperatures read by thermocouple must be similar to setpoint temperature. If thermocouple read a temperature below the setpoint, the temperature controller would actuate induction heating power supply to apply more power to compensate the temperature drop. Having said that induction heating supplies heat internally on the contrary to conventional external heaters, if the bed was at defluidization state, heat would not be transferred uniformly from surface of the metal rods to the bed and would accumulate locally while induction heating would keep delivering power. As a result, temperature would increase.

To develop the observation in Figure 12, temperature profiles during coal combustion with sorbents X_2 and X_3 at temperature of 900°C are illustrated in Figure 13 where Ca and Na with different mass ratios over sulphur content of coal were tested. As presented in Figure 13, after reactor was heated up to setpoint temperature, bed temperature varied around the setpoint indicating heat was uniformly transferred. However, when feed was injected to the reactor, different scenarios were observed with respect to presence of additives in the feed (arrows show the moment coal was injected):

When calcium bearing sorbent X_2 was added to coal, temperature profile stayed around setpoint temperature of 900°C after feed was injected to the bed for all $\frac{Ca+Na/2}{S}$ ratios indicating that the bed was uniformly fluidized and no agglomeration occurred. The observations in Figure 13 were verified at the end of the tests: after heating was shut off and reactor cooled down, no agglomeration was visible despite a thin layer of solids sticked to the rods.

Presence of sodium resulted in a different behavior of temperature profile when an equivalent mixture of sorbents X_2, containing Ca, and X_3, containing Na, were added to coal. A seen in Figure 13, around 40 s after the feed was injected into the reaction zone, bed temperature started to increase indicating development of agglomerates. The temperature increase is attributed to presence of sodium in sorbent X_3 because no defluidization was observed when sorbent X_2 was used only (Figure 13, left hand side).

As expected, larger presence of sodium, which corresponds to larger ratio of $\frac{Ca+Na/2}{S}$, caused significantly higher temperature increase indicating more severe defluidization state.

Results in Figure 13 coincide with reports in literature. This unique feature of the IHFBR makes minimize concern over the defluidization state prediction in large scale fluidized bed reactors.

Further Applications of IHFBR for Kinetics Studies

The IHFBR enables one to perform a wide range of other thermal and catalytic reactions such as pyrolysis and gasification of the solid feedstocks. Since wall of the reaction zone is made of alumina and platinum rods could be used, even extremely high temperature reactions such as pulverized coal combustion at 1500°C can be carried out.

Despite unique feature of the lift tube, the IHFBR has potential to be used also as a fluidized bed TGA for screening tests and kinetics studies. In conventional TGAs, depending on the composition of the solid feedstock, heating rates from 5°C/min to 200°C/min are used for thermal decomposition. The induction heating mechanism lets perform reaction tests in which heating rates from 10°C/min to 100°C/s are interested to be investigated. In such cases, the lift tube does not need to be necessarily used because the solid feedstock

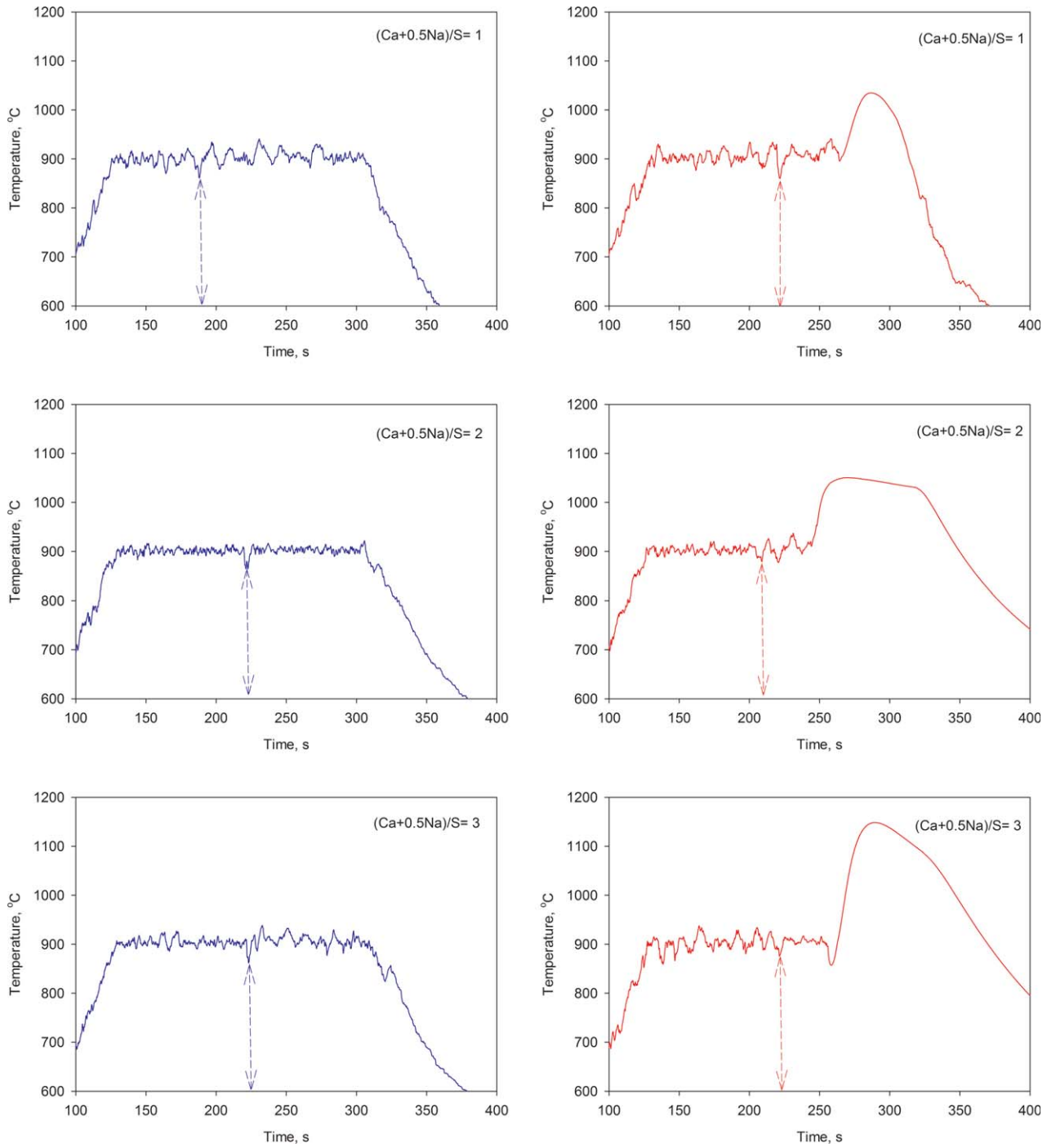

Figure 13. Defluidization monitoring in the reaction zone of the IHFBR: temperature profile during coal combustion assisted with Left: calcium bearing sorbent X_2 and Right: equal mass of calcium bearing sorbent X_2 and sodium bearing sorbent X_3; arrows show the time when feed was injected.

[Color figure can be viewed in the online issue, which is available at wileyonlinelibrary.com.]

can be placed on top of the lift tube and mixed with non-feedstock particles of the fluidized bed. Further investigation is in progress to use the IHFBR as a fluidized bed TGA by precise measurement of the total outlet flow rate.

Conclusion

The Induction Heating Fluidized Bed Reactor (IHFBR) operates similar to conventional fluidized bed reactors in which the lift tube plays role of the gas distributor unconventionally. Bed material in the fluidized bed can vary between the Geldart's group A and group B powders; however, proper type and size distribution must be specified for a target reaction to avoid having significant particles entrainment and particles agglomeration.

The IHFBR can be used for screening and kinetics studies of high temperature reactions such as pyrolysis, gasification, and combustion of solid feedstocks up to 1500°C. This reactor addresses two serious limitations in conventional mini fluidized bed reactors: a very fast heating rate and precise

solid feedstock feeding; as a result, it mimics the exact scenario of feeding cold feedstock to an industrial reactor. The cold feedstock is injected to the fluidized bed through the lift tube within 1 s so that its temperature at the inlet to the reaction zone is reasonably low and no prethermal decomposition occurs on. After the feedstock is injected to the bed, solid particles reach reaction temperature within 3 to 5 s due to the used induction heating mechanism.

Investigation of fluidization quality revealed that although gas from the lift tube with 0.95 cm diameter enters the reaction zone with 2.5 cm diameter, a fluidized bed similar to conventional fluidized beds with a uniform gas holdup is achieved in the IHFBR and there is no defluidized spot in the bed.

Coal combustion tests with the IHFBR resulted in reproducible and expected data. More importantly, this mini reactor is an ideal system to predict defluidization state. Besides, preheating and postreaction cooling-down steps are very fast since an induction heating system is used. Putting all these features together, a complete reaction test within an hour is accomplished while low mass of the feedstock is required, that is, less than 1 g. Therefore, considerable amount of cost is saved and many tests within a short period of time can be carried out.

Acknowledgments

Authors sincerely thank Accordant Energy™ for financial support of this research. The authors are also thankful to Ph.D. students Mr. Jaber Shabanian and Mr. Amin Esmaeili for providing the OFP setup and their supplementary comments.

Notation

A = heat transfer area in the lift tube, m^2
$C_{p,f}$ = heat capacity of the feedstock, J/mol K
d = reference depth, m
f = frequency of an alternative electrical current
h = heat transfer coefficient in the lift tube, W/m^2 K
ΔH = bed height above the lift tube, m
I = Eddy currents induced on a work piece in a magnetic field, A
m_f = mass of the feedstock, kg
ΔP = pressure drop within a bed segment, Pa
ΔP_{max} = weight of the initial bed inventory before solids enter the bed from the lift tube, Pa
r = electrical resistivity, Ω
R = radial distance from center of the reaction zone, m
R_0 = radios of the reaction zone, m
Δt = lifting time in the lift tube, s
T_0 = temperature of the fluidized bed at room temperature, K
T_{bed} = temperature of the fluidized bed, K
T_f = temperature of the feedstock, K
$T_{f,0}$ = initial temperature of the feedstock, K
T_l = temperature inside the lift tube, K
u : = an arbitrary parameter to simplify Eq. 3
U = superficial gas velocity, m/s
U_0 = superficial gas velocity at room temperature, m/s
U_{mf} = minimum fluidization gas velocity, m/s
V = real-time voltage measured by the OFP, V
V_0 = calibrated voltage for the OFP measurements corresponding to an empty reactor, V
V_{mf} = calibrated voltage for the OFP measurements corresponding to minimum fluidization state, V
x_l = length of the lift tube, m
X_i = sorbent i
ε = bed voidage associated with a bed segment estimated using pressure transducer data
ε_{loc} = local bed voidage (average of the recorded real-time local bed voidage at the associated local)
ε_{mf} = bed voidage at minimum fluidization state
$\varepsilon_{r,loc}$ = real-time local bed voidage estimated by OFP data
μ = relative magnetic permeability, m
ρ_p = density of particles, kg/m^3
ρ_g = density of gas, kg/m^3

Literature Cited

1. Latifi M. *Gasification of Bio-Oils to Syngas in Fluidized Bed Reactors* [Ph.D. thesis]. London, Ontario: Chemical and Biochemical Engineering, Western University; 2012.
2. Latifi M, Berruti F, Briens C. Non-catalytic and catalytic steam reforming of a bio-oil model compound in a novel "Jiggle Bed" reactor. *Fuel*. 2014;129:278–291.
3. Latifi M, Berruti F, Briens C. A novel fluidized and induction heated microreactor for catalyst testing. *AIChE J*. 2014;60(9):3107–3122.
4. Ebrahimpour O, Chaouki J, Dubois C. Diffusional effects for the oxidation of SiC powders in thermogravimetric analysis experiments. *J Mater Sci*. 2013;48(12):4396–4407.
5. Samih S, Chaouki J. Development of a fluidized bed thermogravimetric analyzer. *AIChE J*. 2015;61:84–89.
6. Yu J, Yue J, Liu Z, Dong L, Xu G, Zhu J, Duan Z, Sun L. Kinetics and mechanism of solid reactions in a micro fluidized bed reactor. *AIChE J*. 2010;56(11):2905–2912.
7. Yu J, Yao C, Zeng X, Geng S, Dong L, Wang Y, Gao S, Xu G. Biomass pyrolysis in a micro-fluidized bed reactor: characterization and kinetics. *Chem Eng J*. 2011;168(2):839–847.
8. Li J, Liu X, Zhou L, Zhu Q, Li H. A two-stage reduction process for the production of high-purity ultrafine Ni particles in a microfluidized bed reactor. Particuology. 2014. in press.
9. Forret A, Hoteit A, Gauthier T. Chemical looping combustion process applied to liquid fuels. Paper presented at: 2009 AIChE Annual Meeting, Nashville, TN, United states.
10. Hoteit A, Forret A, Pelletant W, Roesler J, Gauthier T. Chemical looping combustion with different types of liquid fuels. *Oil Gas Sci Technol*. 2011;66(2):193–199.
11. Hoteit A, Surla K, Yazdanpannah MM, Rifflart S, Gauthier T. Operation of a new 10kW CLC unit with independant solid flow control. Paper presented at: 2010 AIChE Annual Meeting, Salt Lake City, UT, United states.
12. Stainton H, Ginet A, Surla K, Hoteit A. Experimental investigation of CLC coal combustion with nickel based particles in a fluidized bed. *Fuel*. 2012;101:205–214.
13. Imhof P, Baas M, Gonzalez JA. Fluid catalytic cracking catalyst evaluation: the short contact time resid test. *Catal Rev*. 2004;46(2):151–161.
14. Kraemer DW, de Lasa HI. Catalytic cracking of hydrocarbons in a riser simulator. *Ind Eng Chem Res*. 1988;27(11):2002–2008.
15. Kraemer DW, Sedran U, de Lasa HI. Catalytic cracking kinetics in a novel riser simulator. *Chem Eng Sci*. 1990;45(8):2447–2452.
16. Salaices E, Serrano B, DeLasa H. Biomass catalytic steam gasification: Thermodynamics analysis and reaction experiments in a CREC riser simulator. Paper presented at: 2010 AIChE Annual Meeting, Salt Lake City, UT, United states.
17. Rudnev V, Loveless D, Cook RL, Black M. Handbook of Induction Heating. New York, NY, the United States of America: Marcel Dekker, 2002.
18. Davies J. Conduction and Induction Heating. London, United Kingdom: Peter Peregrinus Ltd.; 1990.
19. Zinn S, Semiatin SL. Elements of Induction Heating: Design, Control, and Applications. Polo Alto, CA: Metals Park, OH: Electrical Power Reserach Institute; ASM International; 1988.
20. Fotovat F, Chaouki J, Bergthorson J. Distribution of large biomass particles in a sand-biomass fluidized bed: experiments and modeling. *AIChE J*. 2014;60(3):869–880.
21. Molerus O, Burschka A, Dietz S. Particle migration at solid surfaces and heat transfer in bubbling fluidized beds—II. Prediction of heat transfer in bubbling fluidized beds. *Chem Eng Sci*. 1995;50(5):879–885.
22. Shabanian J, Chaouki J. Local characterization of a gas-solid fluidized bed in the presence of thermally induced interparticle forces. *Chem Eng Sci*. 2014;119:261–273.
23. Shabanian J, Chaouki J. Hydrodynamics of a gas-fluidized bed with thermally induced interparticle forces. *Chem Eng J*. 2015;259:135–152.
24. Cui H, Chaouki J. Effects of temperature on local two-phase flow structure in bubbling and turbulent fluidized beds of FCC particles. *Chem Eng Sci*. 2004;59(16):3413–3422.

25. Cui H, Mostoufi N, Chaouki J. Comparison of measurement technique of local particle concentration for gas-solid fuidization. Fluidization X; May 20–25, 2001; Beijing, China.
26. Cornpo P, Tardos GI, Mazzone D, Pfeffer R. Minimum sintering temperatures of fluidizable particles. *Part Charact.* 1984;1:171–177.
27. Cornpo P, Pfeffer R, Tardos GI. Minimum sintering temperatures and defluidization characteristics of fluidizable particles. *Powder Technol.* 1987;51:85–101.
28. Zhong Y, Wang Z, Guo Z, Tang Q. Defluidization behavior of iron powders at elevated temperature: influence of fluidizing gas and particle adhesion. *Powder Technol.* 2012;230:225–231.
29. Tardos G, Pfeffer R. Chemical reaction induced agglomeration and defluidization of fluidized beds. *Powder Technol.* 1995;85:29–35.
30. Zhu C, Chu S, Tompsett GA, Yang J, Mountziaris TJ, Dauenhauer PJ. ReEngineered feedstocks for pulverized coal combustion emissions control. *Ind Eng Chem Res.* 2014;53(46):17919–17928.
31. U.S. Environmental Protection Agency. National Ambient Air Quality Syandards (NAAQS), Available at: http://www.epa.gov/air/criteria.html. Accessed on December 2014.
32. U.S. Energy Information Administration. Count of Electric Power Industry Power Plants, Available at: http://www.eia.gov/electricity/annual/html/epa_04_01.html. Accessed on December, 2014.
33. Lupianez C, Guedea I, Bolea I, Diez LI, Romeo LM. Experimental study of SO2 and NOx emissions in fluidized bed oxy-fuel combustion. *Fuel Process Technol.* 2013;106:587–594.
34. Bueno-Lopez A, Garcia-Garcia A. Combined SO_2 and NO_x removal at moderate temperature by a dual bed of potassium-containing coal-pellets and calcium-containing pellets. *Fuel Process Technol.* 2005;86(16):1745–1759.
35. Anthony EJ, Granatstein DL. Sulfation phenomena in fluidized bed combustion systems. *Prog Energy Combust Sci.* 2001;27(2):215–236.
36. Jafari R, Bai D. Reengineered feedstock cofiring with coal in a tangential-fired pulverized boiler. Paper presented at: 11th International Conference on Fluidized Bed Technology, CFB 2014, Beijing, China.
37. Bai D, Inventor. Systems and methods for producing engineered fuel feed stocks from waste material. US patent 579997, 2013.
38. Yu C, Tang Z, Zeng L, Chen C, Gong B. Experimental determination of agglomeration tendency in fluidized bed combustion of biomass by measuring slip resistance. *Fuel.* 2014;128(0):14–20.
39. Ma J, Liu D, Chen Z, Chen X. Agglomeration characteristics during fluidized bed combustion of salty wastewater. *Powder Technol.* 2014;253(0):537–547.
40. Liu Z-S, Peng T-H, Lin C-L. Impact of CaO and $CaCO_3$ addition on agglomeration/defluidization and heavy metal emission during waste combustion in fluidized-bed. *Fuel Process Technol.* 2014;118:171–179.
41. Liu Z-S, Peng T-H, Lin C-L. Effects of bed material size distribution, operating conditions and agglomeration phenomenon on heavy metal emission in fluidized bed combustion process. *Waste Manag.* 2012;32(3):417–425.
42. Chiou-Liang L, Jia-Hong K, Ming-Yen W, Shih-Hsien C, Kai-Sung W. Inhibition and promotion: the effect of earth alkali metals and operating temperature on particle agglomeration/defluidization during incineration in fluidized bed. *Powder Technol.* 2009;189(1):57–63.
43. Davidsson KO, Amand LE, Steenari BM, Elled AL, Eskilsson D, Leckner B. Countermeasures against alkali-related problems during combustion of biomass in a circulating fluidized bed boiler. *Chem Eng Sci.* 2008;63(21):5314–5329.
44. Fernandez Llorente MJ, Escalada Cuadrado R, Murillo Laplaza JM, Carrasco Garcia JE. Combustion in bubbling fluidised bed with bed material of limestone to reduce the biomass ash agglomeration and sintering. *Fuel.* 2006;85(14–15):2081–2092.
45. Lin C-L, Wey M-Y. The effect of mineral compositions of waste and operating conditions on particle agglomeration/defluidization during incineration. *Fuel.* 2004;83(17–18):2335–2343.
46. Lin W, Dam-Johansen K, Frandsen F. Agglomeration in bio-fuel fired fluidized bed combustors. *Chem Eng J.* 2003;96(1–3):171–185.
47. Werther J, Saenger M, Hartge EU, Ogada T, Siagi Z. Combustion of agricultural residues. *Prog Energy Combust Sci.* 2000;26(1):1–27.
48. Bartels M, Lin W, Nijenhuis J, Kapteijn F, van Ommen JR. Agglomeration in fluidized beds at high temperatures: mechanisms, detection and prevention. *Prog Energy Combust Sci.* 2008;34(5):633–666.
49. Jing-Dong C, Chiou-Liang L. Inhibition of agglomeration/defluidization by different calcium species during fluidized bed incineration under different operating conditions. *Powder Technol.* 2012;219:165–172.

Manuscript received July 1, 2014, and revision received Dec. 25, 2014.